Contrib Mineral Petrol (1999) 135: 114 – 132

Cliff S.J. Shaw

Dissolution of orthopyroxene in basanitic magma between 0.4 and 2 GPa: further implications for the origin of Si-rich alkaline glass inclusions in mantle xenoliths

Received: 24 August 1998 / Accepted: 2 December 1998

Abstract A large body of recent work has linked the origin of Si-Al-rich alkaline glass inclusions to metasomatic processes in the upper mantle. This study examines one possible origin for these glass inclusions, i.e., the dissolution of orthopyroxene in Si-poor alkaline (basanitic) melt. Equilibrium dissolution experiments between 0.4 and 2 GPa show that secondary glass compositions are only slightly Si enriched and are alkali poor relative to natural glass inclusions. However, disequilibrium experiments designed to examine dissolution of orthopyroxene by a basanitic melt under anhydrous, hydrous and CO_2-bearing conditions show complex reaction zones consisting of olivine, ± clinopyroxene and Si-rich alkaline glass similar in composition to that seen in mantle xenoliths. Dissolution rates are rapid and dependent on volatile content. Experiments using an anhydrous solvent show time dependent dissolution rates that are related to variable diffusion rates caused by the saturation of clinopyroxene in experiments longer than 10 minutes. The reaction zone glass shows a close compositional correspondence with natural Si-rich alkaline glass in mantle-derived xenoliths. The most Si- and alkali-rich melts are restricted to pressures of 1 GPa and below under anhydrous and CO_2-bearing conditions. At 2 GPa glass in hydrous experiments is still Si- and alkali-rich whereas glass in the anhydrous and CO_2-bearing experiments is only slightly enriched in SiO_2 and alkalis compared with the original solvent. In the low pressure region, anhydrous and hydrous solvent melts yield glass of similar composition whereas the glass from CO_2-bearing experiments is less SiO_2 rich. The mechanism of dissolution of orthopyroxene is complex involving rapid incongruent breakdown of the orthopyroxene, combined with olivine saturation in the reaction zone forming up to 60% olivine. Inward diffusion of CaO causes clinopyroxene saturation and uphill diffusion of Na and K give the glasses their strongly alkaline characteristics. Addition of Na and K also causes minor SiO_2 enrichment of the reaction glass by increasing the phase volume of olivine. Olivine and clinopyroxene are transiently stable phases within the reaction zone. Clinopyroxene is precipitated from the reaction zone melt near the orthopyroxene crystal and redissolved in the outer part of the reaction zone. Olivine defines the thickness of the reaction zone and is progressively dissolved in the solvent as the orthopyroxene continues to dissolve. Although there are compelling reasons for supporting the hypothesis that Si-rich alkaline melts are produced in the mantle by orthopyroxene – melt reaction in the mantle, there are several complications particularly regarding quenching in of disequilibrium reaction zone compositions and the mobility of highly polymerized melts in the upper mantle. It is considered likely that formation of veins and pools of Si-rich alkaline glass by orthopyroxene – melt reaction is a common process during the ascent of xenoliths. However, reaction in situ within the mantle will lead to equilibration and therefore secondary melts will be only moderately siliceous and alkali poor.

Introduction

Glass inclusions occur in many mantle xenoliths in a variety of textural settings including isolated inclusions in olivine, clinopyroxene and orthopyroxene (e.g., Schiano and Clocchiatti 1994) and intergranular pools, veins and stringers (e.g., O'Connor et al. 1996; Wilshire and McGuire 1996; Neumann and Wulff-Pedersen 1997). A compilation of published glass analyses (Fig. 1) shows that almost the entire igneous spectrum is represented. Given the wide range of observed compositions and the variety of textural settings, there have been numerous hypotheses put forward to explain the origin of glass inclusions. The hypotheses can be divided into

C.S.J. Shaw
Bayerisches Geoinstitut, Universität Bayreuth,
D-95440 Bayreuth, Germany
E-mail: Cliff.Shaw@uni-bayreuth.de

Editorial responsibility: J. Hoefs

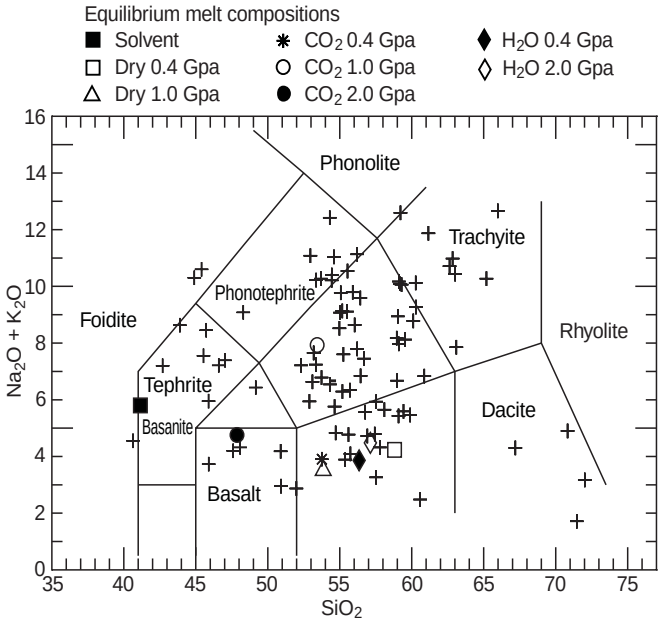

Fig. 1 Range of glass compositions from mantle xenoliths worldwide. (Data sources: Francis 1976a, b; Jones et al. 1983; Gamble and Kyle 1987; Edgar et al. 1989; Hansteen et al. 1991; Draper 1992; Dautria et al. 1992; Ionov et al. 1993; 1994; Schiano and Clocchiatti 1994; Schiano et al. 1994; O'Connor et al. 1996; Yaxley et al. 1997)

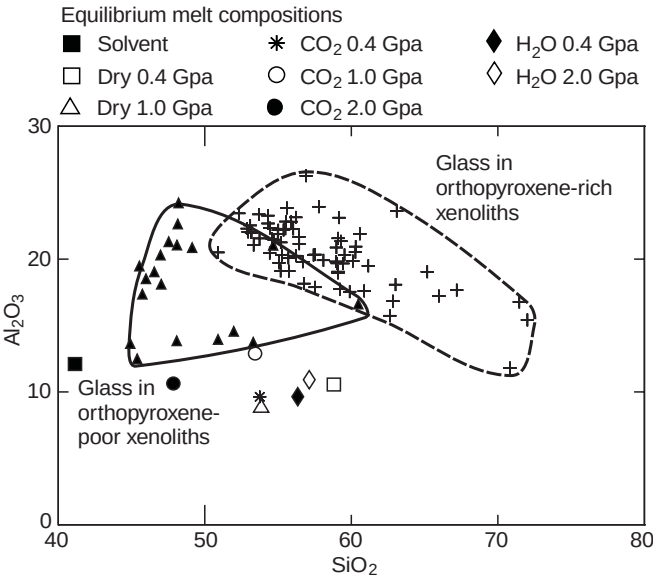

Fig. 2 Comparison of xenolith glass compositions from orthopyroxene-poor and orthopyroxene-rich xenoliths (from Shaw et al. 1998, see Fig. 1 for data sources)

two distinct groups. The first group suggests that glass inclusions are formed during entrainment and transport of the xenoliths to the Earth's surface, e.g., by decompression melting of amphibole, partial melting or reaction during residence in crustal magma chambers or infiltration of the host magma (Frey and Green 1974; Francis 1976a, 1987; Tracy 1980; Shaw and Edgar 1997; Yaxley et al. 1997; Klügel 1998). The second group of hypotheses suggest that glass inclusions, veins and pools are formed at mantle depths and therefore have a direct bearing on mantle processes. This group includes: reaction between peridotite and infiltrating "basaltic" melts (Zinngrebe and Foley 1995; Wilshire and McGuire 1996; Wulff-Pedersen et al. 1996; Neumann and Wulff-Pedersen 1997); partial melting of variably metasomatised mantle (Hauri et al. 1993; Ionov et al. 1994); separation of immiscible melts (Schiano et al. 1994); percolation of slab melts into the overlying depleted mantle wedge (Schiano et al. 1995) and infiltration of metasomatic melts of unknown origin into peridotitic mantle (Edgar et al. 1989; Schiano and Clocchiatti 1994).

An examination of the available data on the modal composition of mantle xenoliths and the associated glass shows that the inclusions, veins and pools can be divided into two distinct groups (Wilshire and McGuire 1996; Yaxley et al. 1997; Shaw et al. 1998). The first group is Si poor and occurs mainly in xenoliths that contain less than 1% orthopyroxene (Fig. 2). The second group is Si rich and occurs in xenoliths containing greater than 1% orthopyroxene. This observation formed the basis for experiments by Shaw et al. (1998) that examined the behavior of orthopyroxene under going dissolution by Si-undersaturated alkaline melts at one atmosphere pressure. The experiments showed that partially reacted orthopyroxene crystals are surrounded by reaction zones that contain very Si rich alkaline glass similar in composition to the Si-rich glasses found in orthopyroxene-rich mantle xenoliths. On the basis of these experiments Shaw et al. (1998) suggested that at least some Si-rich alkaline glass in mantle xenoliths could result from reaction at low pressure during transport and eruption of the host magma.

The objectives of the present study were two fold:

1. To test the hypothesis that Si-rich alkaline glass inclusions are a product of orthopyroxene – melt reaction under mantle pressures (Zinngrebe and Foley 1995; Wulff-Pedersen et al. 1996; Neumann and Wulff-Pedersen 1997).

2. To examine the mechanism of orthopyroxene dissolution using dissolution rate, textural and chemical data. Details of dissolution kinetics and mechanisms are important to further development of models involving reaction during melt transport (e.g., Kelemen 1986; Navon and Stolper 1987; Reiners 1998).

Experimental methods

The experiments were performed using a synthetic basanite melt (Table 1) as a solvent. Glass for anhydrous and hydrous experiments was produced by multiple fusions of the requisite oxides and carbonates at 1350 °C. For CO_2-bearing experiments a separate glass was prepared by fusion of all the oxides and carbonates except K_2CO_3 which was added after fusion to give the required K_2O and CO_2 contents (Table 1). On the basis of CO_2 solubility measurements in a melt of similar composition (Thibault and Holloway 1994) a value of 5% CO_2 was chosen, since at the conditions of the

Table 1 Composition of starting materials used in the equilibrium and dissolution experiments

Wt%	Anhydrous glass	Hydrous glass	CO_2-bearing glass	Opx
SiO_2	41.15	39.50	39.09	57.14
TiO_2	2.74	2.63	2.60	0.04
Al_2O_3	12.10	11.62	11.50	2.85
FeO	10.11	9.71	9.60	5.51
MnO	0.18	0.17	0.17	0.14
MgO	11.24	10.79	10.68	33.10
CaO	15.66	15.03	14.88	0.86
Na_2O	2.76	2.65	2.62	0.09
K_2O	3.04	2.92	2.89	0.00
P_2O_5	1.02	0.98	0.97	0.00
Cr_2O_3	0.00	0.00	0.00	0.76
CO_2	0.00	0.00	5.00	0.00
H_2O	0.00	4.00	0.00	0.00
Total	100.00	100.00	100.00	100.49

experiments this is close to the saturation value, at least at 1 and 2 GPa. The starting glasses were ground under ethanol in an agate mortar and pestle to a grain size of approximately 20 μm and were stored in a drying oven at 150 °C until required.

Inclusion-free enstatite crystals (Table 1) were hand-picked from a very coarse grained spinel lherzolite from San Carlos, Arizona. Approximately 300 grains were selected and ground in a sphere maker (Bond 1951) yielding 40 useable grains that were spherical to within 4 to 8%. These 40 spheres were polished to 4000 grit before use. A few discs of orthopyroxene were cut to size with a diamond wire saw and then polished to 4000 grit. All of the enstatite grains were measured using a microscope-mounted micrometer accurate to 5 μm. Each grain was measured at least ten times on two separate occasions and the average value was used as the starting size.

The experiments were performed in a 3/4-inch piston cylinder apparatus using talc – Pyrex assemblies with a tapered graphite heater. Temperature was monitored by a Pt-$Pt_{90}Rh_{10}$ thermocouple placed on top of the sample capsule and was controlled with a Eurotherm 818P controller. Samples were heated at 200 °C per minute and were quenched by turning off the power to the controller while maintaining sample pressure (i.e., isobaric quench). Measurements made during temperature calibration C.S.J. Shaw and Fliervoet, unpublished data) indicate that 1 cm capsules are exposed to a thermal gradient of approximately 10 °C. Quench rates were between 80 and 100 °C per s.

A digital pressure gauge attached to a transducer on the oil line was used to monitor pressure. All of the samples were cold pressurised to 10–15% above the desired pressure. During heating, the pressure within the sample chamber decreases due to progressive dehydration of the talc. The over-pressure at the run temperature, approximately 5% greater than the final run pressure, was bled off within a minute of reaching run temperature (i.e., hot-piston out). Pressure was calibrated against the albite–quartz–jadeite reaction and the kyanite–sillimanite transition (Holland 1980; Edgar et al. 1988). On the basis of these measurements a 20% friction correction was applied.

Samples were contained in iron-soaked platinum capsules for experiments of less than 30 minutes duration and in graphite-lined platinum capsules for experiments longer than 30 minutes. The capsules were tightly packed with glass powder and a sphere or disc of enstatite was placed on top and covered with more tightly packed glass powder. For the water-bearing experiments, the required amount of water was added by microsyringe. To ensure that water was retained during sealing of the capsules they were partly immersed in water and had a piece of wet tissue wrapped around them during welding. Water-bearing capsules were weighed before and after welding and then after 2–4 hours in a drying oven at 150 °C. Any capsule that showed weight loss was discarded.

Phase equilibria of the solvent melts

The near liquidus phase relations of the anhydrous solvent melt are based on a series of 12 experiments (Table 2) carried out between 1 atmosphere and 2.5 GPa. The results of the experiments are presented in Fig. 3. All subliquidus experiments crystallized clinopyroxene. These data were used to select the temperatures for the dissolution experiments. To avoid complications due to the presence of solid phases in the solvent melt all the experiments were done at temperatures just above the liquidus (Fig. 3).

Precise phase relations of the H_2O- and CO_2-bearing melts proved impossible to obtain. All of the samples were affected by extreme quench crystallization and it was impossible to determine if crystals were equilibrium or quench. It was therefore decided that all the dissolution experiments would be run at the temperatures chosen based on the anhydrous phase equilibria. At these temperatures the water- and carbon dioxide-bearing solvent melts would have had a large amount of superheat due to the depression of the liquidus by the volatile phase. This depression relative to the liquidus of the anhydrous solvent is pressure dependant (Fig. 3) and varies from 70 to 130 °C for the water-bearing solvent (based on modeling using MELTS software, Ghiorso and Sack 1995).

Equilibration experiments

In-situ reaction of orthopyroxene and an infiltrating silicate melt will likely lead to equilibrium and thus to saturation of the infiltrating magma with orthopyroxene. Therefore, as a first test of the viability of orthopyroxene – melt reaction in the formation of Si-Al-rich alkaline glass inclusions several experiments were done with 40% melt (anhydrous, hydrous and CO_2-bearing) intimately mixed with 60% finely ground San Carlos enstatite. These equilibration experiments were carried out at the pressure and temperature conditions chosen on the basis of the phase equilibria runs and were of at least 24 hours duration (Table 2).

Analytical methods

Dissolution rates (Table 2) were obtained by measuring the maximum size of the enstatite spheres before and after each experiment. After the experiments, the capsules were set in epoxy plugs and ground open. When the enstatite sphere was intercepted, its size was measured, with subsequent measurements being made after 10 seconds of grinding using 500 grit abrasive. This removes approximately 10 microns of material when the abrasive is new and about 6 microns when the abrasive has been used for several grindings. This sequence was done for all of the experiments until the maximum sphere diameter was obtained. For experiments where discs rather than spheres were used, the size of the disc was measured at several points along its length and at several places within the diameter of the capsule. Estimated errors for dissolution rates based on multiple measurements of spheres before each experiment and the errors associated with grinding after each experiment are approximately 10% of the measured value.

The starting materials and run products were analyzed with a Cameca SX-50 electron microprobe operating at an accelerating voltage of 15 kV and a using a beam current of 10 nA for a beam 4 μm in diameter. Regions of quench crystals were analyzed with a 10–20 μm diameter beam. To reduce alkali migration and "grow-in" of silica due to heating of the sample by the electron beam, short counting times (20 s) were used and Na, K and Si were counted early in the analysis. A range of natural and synthetic materials was used for standardization and all data were reduced using the PAP correction routine.

Table 2 Experimental conditions and results. Experiments highlighted in *italics* were performed using discs rather than spheres of orthopyroxene (*opx*). (*Phase eq* phase equilibrium experiment, *equilib* equilibration experiment, *dissol* dissolution experiment, *Initial r* initial radius of opx sphere, *Final r* final radius of opx sphere, *Delta r* change in radius of opx sphere, *D* completely dissolved, *cpx* clinopyroxene, *ol* olivine). Duration of experiments is in hours

Experiment	Type	Volatile	*P* (GPa)	*T* (°C)	Duration	Comments		
DLC-12	Phase eq	None	1 bar	1250	1	Glass		
DLC-13	Phase eq	None	1 bar	1225	1	Glass + cpx		
DLC-14	Phase eq	None	1 bar	1200	1	Glass + cpx		
DLC-1	Phase eq	None	1.0	1250	4	Glass + cpx + quench ol		
DLC-2	Phase eq	None	1.0	1295	2	Glass + cpx		
DLC-3	Phase eq	None	1.0	1330	2	Glass		
DLC-5	Phase eq	None	1.0	1340	2	Glass		
DLC-6	Phase eq	None	2.0	1420	2	Glass		
DLC-7	Phase eq	None	2.0	1410	2	Glass + cpx		
DLC-8	Phase eq	None	2.0	1430	1	Glass		
DLC-10	Phase eq	None	2.5	1462	1	Glass cpx		
DLC-11	Phase eq	None	2.5	1474	1	Glass		
OPX-3	Equilib	None	0.4	1280	42			
OPX-1	Equilib	None	1.0	1348	28			
OPX-2	Equilib	None	2.0	1442	25			
OPX-6	Equilib	H_2O	0.4	1280	24			
OPX-4	Equilib	H_2O	1.0	1348	24			
OPX-5	Equilib	H_2O	2.0	1442	24			
OPX-9	Equilib	CO_2	0.4	1280	24			
OPX-7	Equilib	CO_2	1.0	1348	24			
OPX-8	Equilib	CO_2	2.0	1442	24			
						Initial r (mm)	Final r (mm)	Delta r (mm)
97-op1a	Dissol	None	0.4	1280	0.083	0.3800	0.3750	0.0050
97-op1b	Dissol	None	0.4	1280	0.083	0.4530	0.4380	0.0150
97-op-2a	*Dissol*	*None*	*0.4*	*1280*	*0.166*	*0.4010*	*0.3550*	*0.0460*
97-op2b	Dissol	None	0.4	1280	0.166	0.3545	0.2950	0.0595
97-op-26	Dissol	None	0.4	1280	0.333	0.6375	0.5500	0.0875
97-op-3a	Dissol	None	0.4	1280	0.500	0.7320	0.6150	0.1170
97-op-4	Dissol	None	0.4	1280	1.250	0.7615	0.5705	0.1910
97-op-5	Dissol	None	0.4	1280	2.000	1.4940	1.2850	0.2090
97-op-6a	Dissol	None	1.0	1348	0.083	0.4820	0.4100	0.0720
97-op-6b	Dissol	None	1.0	1348	0.083	0.4500	0.4250	0.0250
97-op-21b	Dissol	None	1.0	1348	0.166	0.3500	0.2100	0.1400
97-op-8a	Dissol	None	1.0	1348	0.500	0.6925	0.4225	0.2700
97-op-8b	*Dissol*	*None*	*1.0*	*1348*	*0.500*	*0.7350*	*0.4750*	*0.2600*
97-op-27	Dissol	None	1.0	1348	0.500	0.7150	0.4800	0.2350
97-op-9	Dissol	None	1.0	1348	1.000	1.0500	0.6700	0.3800
97-op-10	Dissol	None	1.0	1348	2.000	1.1500	0.7400	0.4100
97-op-11a	Dissol	None	2.0	1442	0.000	0.3050	0.3050	0.0000
97-op-11b	Dissol	None	2.0	1442	0.000	0.3850	0.3850	0.0000
97-op-12a	Dissol	None	2.0	1442	0.166	0.3800	0.3350	0.0450
97-op-18b	*Dissol*	*None*	*2.0*	*1442*	*0.166*	*0.5750*	*0.5100*	*0.0650*
97-op-13a	Dissol	None	2.0	1442	0.500	0.9000	0.6750	0.2250
97-op-14	Dissol	None	2.0	1442	1.000	0.8450	0.4650	0.3800
97-op-15	Dissol	None	2.0	1442	2.000	0.9105	0.2905	0.6200
97-op-34	Dissol	H_2O	1.0	1348	0.500	0.6120	0.3110	0.3010
97-op-23b	Dissol	H_2O	1.0	1348	0.750	1.5225	0.8980	0.6245
97-op-16	Dissol	H_2O	1.0	1348	2.000	1.0145	D	1.0145
97-op-19b	Dissol	H_2O	2.0	1442	0.500	0.9845	0.5300	0.4545
97-op-20b	Dissol	H_2O	2.0	1442	0.750	1.3795	0.6775	0.7020
97-op-17	Dissol	H_2O	2.0	1442	2.000	0.8750	D	0.8750
97-op-21a	Dissol	CO_2	1.0	1348	0.166	0.4825	0.4125	0.0700
97-op-24	Dissol	CO_2	1.0	1348	1.000	0.6925	0.4510	0.2415
97-op-18a	Dissol	CO_2	2.0	1442	0.166	0.5750	0.5350	0.0400
97-op-19a	Dissol	CO_2	2.0	1442	0.500	0.8180	0.6950	0.1230
97-op-20a	Dissol	CO_2	2.0	1442	0.750	0.7325	0.5550	0.1775
97-op-25	Dissol	CO_2	2.0	1442	1.000	0.7200	0.5350	0.1850

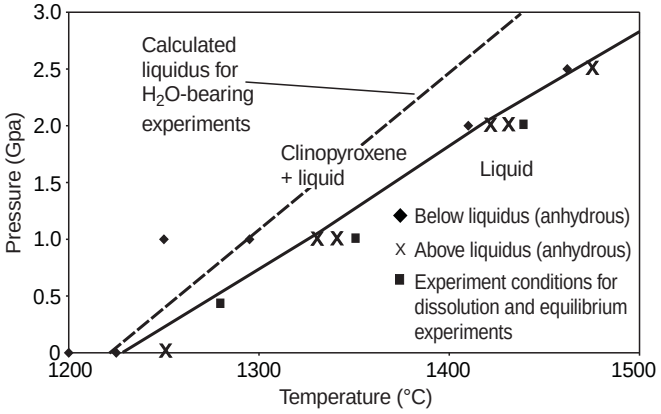

Fig. 3 Near liquidus phase relations of anhydrous basanite melt (*solid line*) determined from experiment. The *dashed line* shows the liquidus curve for basanite + 5% H_2O. This curve was calculated using the MELTS program of Ghiorso and Sack (1995)

Results

Equilibration experiments

In order to obtain secondary glass compositions from the equilibration experiments, which used a mixture of 40% solvent melt and 60% orthopyroxene, all the phases present (equilibrium and quench) were analyzed and their proportions estimated by point counting several backscattered electron photomicrographs. To examine the effects of quench crystallization on the secondary glass compositions, mass balance calculations were carried out using the measured modes and analyzed compositions. Where required, the composition of obvious quench crystals was added to the analyzed glass before performing the mass balance calculations. The results of the calculations are given in Table 3. The glass compositions given are those calculated; the difference column for each analysis represents the difference between the calculated glass composition and that actually measured by microprobe. For all the experiments the glass compositions were calculated on an anhydrous basis. The difference between calculated and analyzed glass compositions is generally small. However, for OPX-1 and OPX-5 the differences are large, suggesting that the glass composition was strongly affected by quench crystallization. Glass compositions for experiments under dry conditions at 2 GPa and hydrous conditions at 1 GPa are not reported since the analysis/mass balance approach gave widely different compositions that were impossible to evaluate with any degree of confidence.

In the anhydrous equilibration experiments the crystalline phases are orthopyroxene and olivine (Table 3). With increasing pressure, the percentage of melt increases at the expense of orthopyroxene which was almost completely consumed in the 1 GPa experiment. There is a minor decrease in the SiO_2 content of the glass at 1 GPa compared to 0.4 GPa. Although more ortho-

Table 3 Glass compositons from equilibration experiments

Sample	OPX-3[a]	Diff[b]	OPX-1	Diff	OPX-6	Diff	OPX-5	Diff	OPX-9	Diff	OPX-7	Diff	OPX-8	Diff
P(GPa)	0.4		1		0.4		2		0.4		1		2	
Volatile	None		None		H_2O		H_2O		CO_2		CO_2		CO_2	
Wt%														
SiO_2	54.59	−0.22	53.53	−0.26	56.08	0.09	56.68	−0.45	53.51	−0.27	52.65	−0.21	47.60	−0.35
TiO_2	1.89	0.07	1.59	0.06	1.75	−0.02	1.99	−0.10	1.72	−0.03	2.24	0.08	2.49	0.07
Al_2O_3	10.52	0.75	8.74	−3.16	9.59	−0.69	10.83	−1.78	9.58	−0.19	12.70	−0.90	10.58	−0.85
FeO	6.73	−0.81	7.97	2.73	6.28	0.47	6.63	1.20	6.68	−0.23	7.85	−0.12	9.53	0.50
MnO	0.16	0.00	0.16	0.00	0.16	0.01	0.17	0.03	0.15	0.01	0.14	−0.04	0.21	0.04
MgO	9.92	0.09	14.31	−0.41	11.01	−0.24	6.28	−0.24	13.67	−0.01	8.09	−0.08	14.64	−0.26
CaO	11.26	−0.58	9.63	0.51	10.68	0.06	12.25	0.67	10.17	0.18	7.24	0.12	9.19	0.02
Na_2O	2.07	0.25	1.71	0.22	1.89	0.18	2.19	0.46	1.91	0.21	3.67	0.84	1.70	0.05
K_2O	2.14	0.33	1.77	0.28	1.95	0.08	2.25	0.16	1.97	0.16	4.15	0.61	3.03	−0.01
P_2O_5	0.72	0.13	0.59	0.04	0.62	0.05	0.72	0.04	0.64	0.17	1.27	0.62	1.02	0.48
Total	100.00		100.00		100.00		100.00		100.00		100.00		100.00	
Modal %														
Glass	56.9		69.5		60.0		51.6		61.6		21.4		33.7	
Clinopyroxene	11.0		1.5		2.0		6.0		10.9		18.8		31.3	
Olivine	32.1		29.0		38.0		42.4		27.4		23.0		10.4	
Clinopyroxene	0.0		0.0		0.0		0.0		0.0		36.8		24.6	

[a] Compositions given are calculated on the basis of mass balance using the modes
[b] (*Diff* difference between calculated glass composition and that analyzed by microprobe)

pyroxene was consumed at the higher pressure, the silica content of the melt decreased since less olivine crystallized. The lower Al_2O_3, CaO, Na_2O and K_2O and higher FeO and MgO of the secondary glass at 1 GPa are also due to the large amount of orthopyroxene consumed and the smaller amount of olivine crystallized.

In the hydrous equilibration experiments, orthopyroxene contents are low (Table 3), indicating a high solubility under these conditions. However, the residual orthopyroxene content increases with pressure. The proportion of melt decreases with increasing pressure while the percentage of olivine increases which results in a small enrichment of the glass in SiO_2 with increasing pressure, whereas the MgO content of the glass decreases due to the higher proportion of olivine crystallized at higher pressure; CaO and the alkalis increase for the same reason.

The CO_2-bearing equilibration experiments show a general increase in the proportion of residual orthopyroxene with increasing pressure. Olivine content decreases with increasing pressure and clinopyroxene appears as a stable phase at 1 GPa and above. The SiO_2 content of the secondary melts at 0.4 and 1 GPa are similar but the 2 GPa melt is much less siliceous since there was much less orthopyroxene dissolved and clinopyroxene crystallization will tend to decrease the SiO_2 content of the melt.

The compositions of the secondary melts in the equilibration experiments are consistent with direct mixing between orthopyroxene and solvent with extraction of olivine, and in the CO_2-bearing experiments at 1 and 2 GPa, clinopyroxene (Table 3).

Comparison of the composition of the secondary melts with those found in nature shows that although there is some overlap, the melts formed by equilibration of the Si-undersaturated solvent with orthopyroxene do not extend to such high SiO_2, Al_2O_3 or alkali contents as natural xenolith glasses (Figs. 1 and 2).

The results of the equilibration experiments indicate that while some moderately Si- and alkali-rich glass inclusions may have formed by equilibration between infiltrated Si-undersaturated melt and orthopyroxene, there is a broad range of natural glass compositions that cannot be explained by this process.

Dissolution experiments

The bulk of the experiments reported here were performed to assess the behavior of orthopyroxene during dissolution. In all the experiments the charge was quenched prior to the attainment of equilibrium.

Dissolution rates

Dissolution rates of orthopyroxene were determined for anhydrous solvent melt at 0.4, 1 and 2 GPa and for hydrous and CO_2-bearing solvent at 1 and 2 GPa (Table 2, Fig. 4). Volatile-bearing dissolution experiments were not done at 0.4 GPa since equilibrium experiments indicated that there was only a minor difference in the compositions of the products between 0.4 and 1 GPa (Table 3). Experiment durations varied from 0 to 120 minutes. The "zero time" experiments were performed to examine the effect of the heating ramp on dissolution. There was no observable dissolution of orthopyroxene in these experiments. Thus, a heating rate of 200 °C per minute did not appear to affect the dissolution rate measurements.

Figure 4 shows a comparative plot of the change in sphere radii with time for each set of experiments. The anhydrous dissolution rates are apparently time dependent and are best fitted with a power law function of the form $y = ax^b$ with the coefficients a and b being distinct for each pressure. These lines were fitted by forcing a 0,0

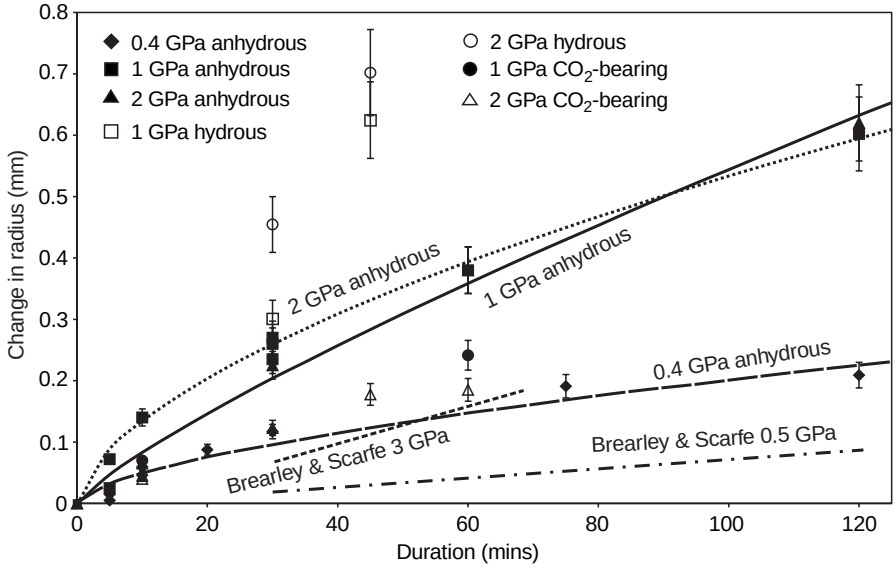

Fig. 4 Dissolution rate data for anhydrous, hydrous and CO_2-bearing dissolution experiments. Brearley and Scarfe data taken from Brearley and Scarfe (1986). Error *bars* on data points correspond to 10% error

intercept since at zero time there was no dissolution. Figure 4 shows that the dissolution rates at 1 and 2 GPa are much faster than at 0.4 GPa under anhydrous conditions which is in accordance with previous observations of increasing dissolution rate with increasing pressure (Brearley and Scarfe 1986). The observed dissolution rate at 2 GPa is only slightly faster than at 1 GPa and in the longest duration experiments there is no discernable difference in the dissolution rate.

Addition of H_2O to the solvent melts results in faster dissolution at 1 and 2 GPa likely because of the larger degree of superheat imposed on the solvent and the fluxing effect of water. Addition of CO_2 to the solvent decreases the dissolution rate at 1 and 2 GPa relative to the anhydrous solvent. However, the observed rate is faster at 1 GPa than at 2 GPa.

In several experiments enstatite discs were used in place of spheres. The measured dissolution rates in these experiments agree with those determined from the sphere dissolution runs (Table 2) indicating that the initial shape of the orthopyroxene and interface kinetics do not play a major role in determining dissolution rates. Additional evidence for this comes from the observation that initially disc shaped enstatite grains develop a rounded rather than faceted morphology (cf. Donaldson 1985).

Textural features of anhydrous experiments

At 0.4 GPa, partially dissolved orthopyroxene crystals are surrounded by a reaction zone consisting of olivine and glass ± clinopyroxene (Table 4, Fig. 5). Olivine is elongate and oriented normal to the orthopyroxene edge and defines the width of the reaction zone. The olivine grains decrease in size and become more rounded with increasing distance from the orthopyroxene interface (Fig. 5a, b).

In the shortest duration experiments clinopyroxene is absent whereas in experiments of 10 minutes or longer there is subhedral clinopyroxene enclosing olivine at the interface between the reaction zone and orthopyroxene (Fig. 5a). In experiments longer than 30 minutes clinopyroxene forms a distinct boundary between two regions that contain different glass compositions (Fig. 5b). Clinopyroxene close to the orthopyroxene – melt interface has a well-developed faceted morphology; whereas that on the outer margin, closest to the solvent, has ragged or rounded faces suggesting that it was undergoing dissolution (Fig. 5b).

At 1 GPa, short duration experiments consist of olivine and glass, at longer durations clinopyroxene is an integral part of the reaction zone but is again limited to the inner part (Fig. 5c) where it separates two regions of glass with distinct composition. Again, the texture of clinopyroxene varies from faceted near the orthopyroxene – melt interface to rounded on the outer side. As in the 0.4 GPa experiments olivine is elongate and oriented normal to the orthopyroxene and its grain size decreases

Table 4 Estimated modal mineralogy of reaction zones around orthopyroxene (*q* quench crystallised, material appears similar to clinopyroxene)

Sample	1a	2a	op4	op21b	op8a	op9	op10	op12a	op13a	op14	op15	op21a	op24	op19a	op20a	op25	op34
P (Gpa)	0.4	0.4	0.4	1	1	1	1	2	2	2	2	1	1	2	2	2	1
T (°C)	1280	1280	1280	1348	1348	1348	1348	1442	1442	1442	1442	1348	1348	1442	1442	1442	1348
Volatile	None	None	None	None	None	None	None	None	None	None	None	CO_2	CO_2	CO_2	CO_2	CO_2	H_2O
Duration (min)	5	10	75	10	30	60	120	10	30	60	120	45	60	30	45	62	30
Olivine	43	60	42	48	37	25	47	39	22	46	45	38	42	42	38	19	47
Clinopyroxene	0	14	23	0	47	31	25	50	78	42	55	62	58	58	62	81	0
Glass	57	26	35	52	16	44	28	11	q	12	q	q	q	q	q	q	53
Total	100	100	100	100	100	100	100	100	100	100	100	100	100	100	100	100	100

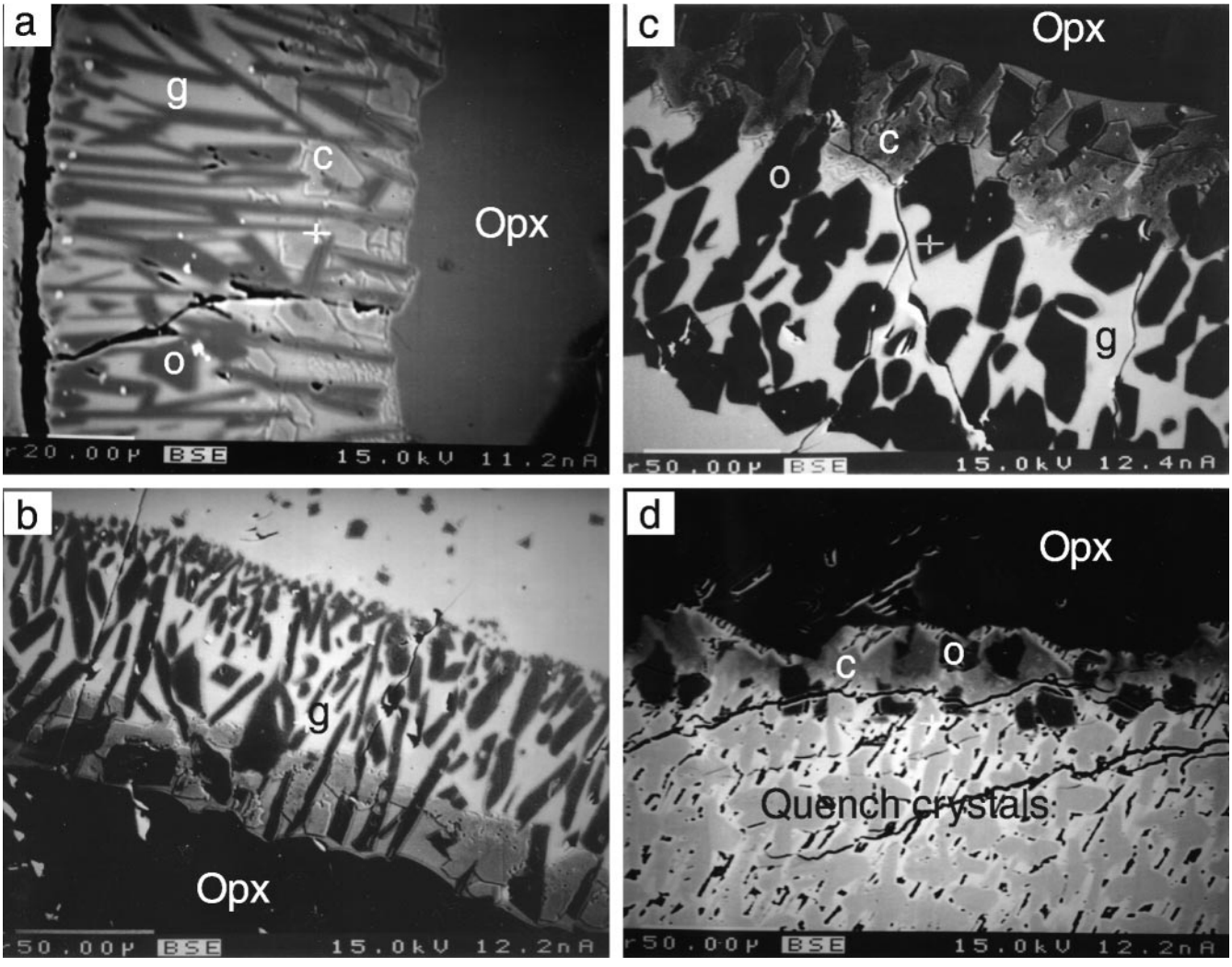

Fig. 5a–d Backscatter electron micrographs of reaction zone textures in anhydrous dissolution experiments: **a** Sample 97-op-2b (0.4 GPa, 10 min) showing elongate olivine crystals with small subhedral clinopyroxene crystals clustered near the margin of the orthopyroxene. The remainder of the material is variably siliceous glass. **b** Sample 97-op-4 (0.4 GPa, 75 min) showing elongate olivine crystals whose grain size decreases outward. Note that the subhedral clinopyroxene crystals separate glass of widely different composition. **c** Sample 97-op-10 (1 GPa, 2 h) reaction zone consisting of sub- to euhedral olivine with an inner region of clinopyroxene that separates glass of distinctive composition. **d** Sample 97-op-14 (2 GPa, 1 h) reaction zone consisting of olivine and clinopyroxene. The feathery material in the reaction zone is quenched glass. In addition, all the solvent outside the reaction zone has been affected by intense quench crystallization

outward although this effect is not as pronounced as in the 0.4 GPa experiments.

At 2 GPa, the texture of the reaction zone is distinct from that found in the lower pressure runs. Olivine is generally less abundant and most of the reaction zone consists of clinopyroxene with a small amount of residual glass (Table 4, Fig. 5d). The boundary between the reaction zone and the solvent is difficult to detect due to quench crystallization of the solvent and reaction zone glasses. The increase in the percentage of clinopyroxene at the expense of glass in the 2 GPa experiments (Table 4) suggests a change in the phase relations of the system. However, the exact proportion of equilibrium clinopyroxene is difficult to determine due to the quench crystallization that is ubiquitous in these samples.

The presence of clinopyroxene in the reaction zones of dry dissolution experiments (Table 4) contrasts with the observations made in the equilibration experiments (Table 3).

Textural features of H_2O-bearing dissolution experiments

The only crystalline phase in the reaction zone of 1 GPa water-bearing experiments is olivine (Table 4, Fig. 6a). As in the anhydrous experiments olivine is elongate and is oriented normal to the orthopyroxene margin and generally decreases in size outward. Glass forms the interstices between the olivine crystals and is occasionally included within them. Much of the glass in the region closest to the enstatite has been affected by quench crystallization. However, pristine glass is preserved farther out toward the solvent and the solvent itself only shows quench crystallization at the capsule walls.

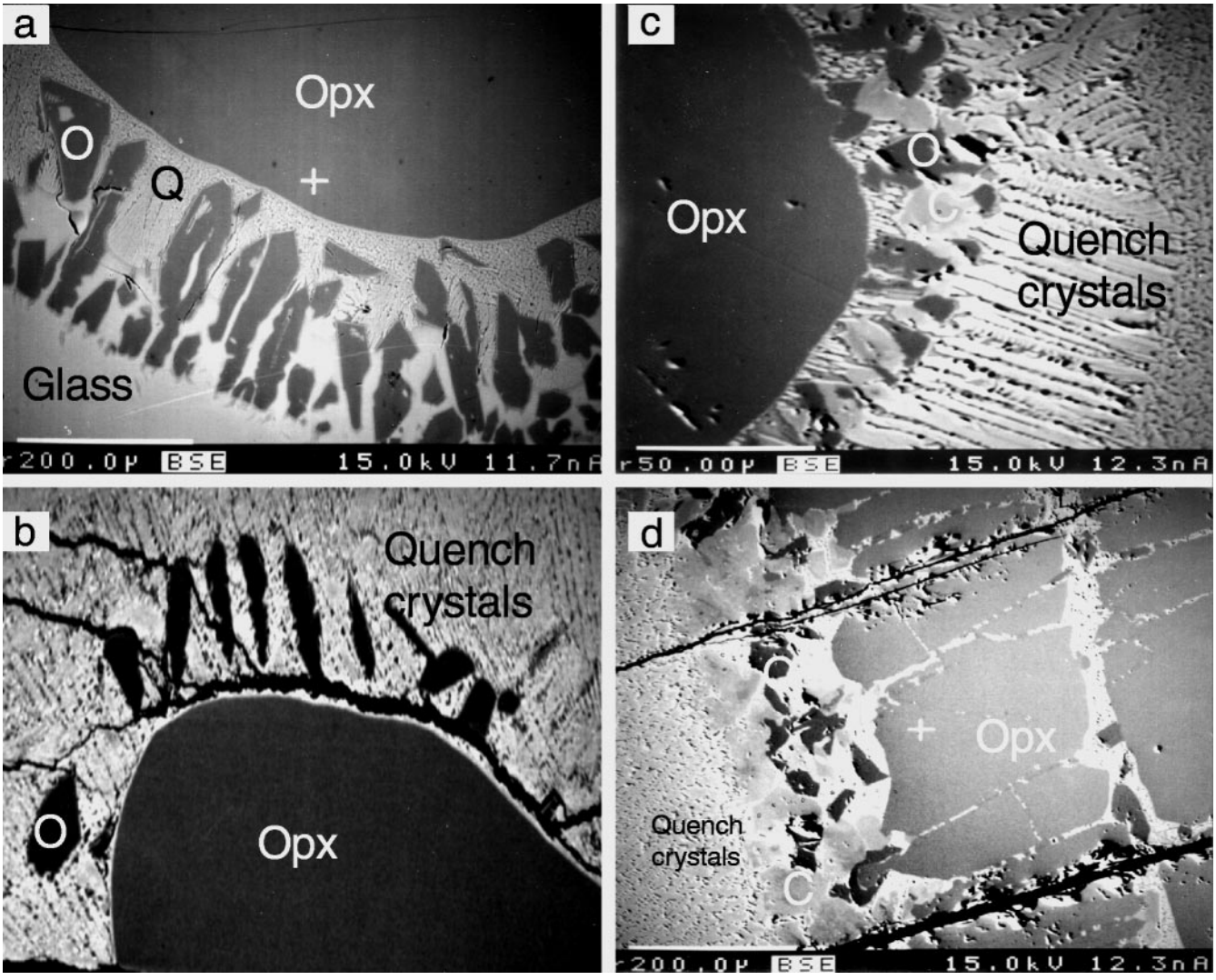

Fig. 6a–d Backscatter electron micrographs of textures in hydrous and CO_2-bearing dissolution experiments: **a** Sample 97-op-34 (1 GPa, 30 min, hydrous) reaction zone consisting of elongate olivine crystals that decrease in size away from the orthopyroxene margin. Note the presence of quench crystallized material at the boundary of the orthopyroxene grain. **b** Sample 97-op-19b (2 GPa, 30 min, hydrous) reaction zone containing olivine. All of the melt phase has crystallized to form a network of quench crystals (note that this photograph has been stretched by 25% in the *x* direction in order to show the most detail). **c** Sample 97-op-24 (1 GPa, 1 h, CO_2 bearing) reaction zone consisting of olivine and zoned clinopyroxene with abundant quench crystals both in the reaction zone and the surrounding solvent. **d** Sample 97-op-25 (2 GPa, 1 h, CO_2 bearing) reaction zone consisting of olivine and clinopyroxene with interstitial patches of quench crystals. The *large fracture* on the orthopyroxene on the *right side* of the photograph probably developed during cold pressurization of the sample. Note that the solvent in this sample has undergone quench crystallization

In contrast to the 1 GPa experiments quench crystallization of the reaction zone glass and the solvent is a serious problem in 2 GPa runs (Fig. 6b). Nevertheless, the reaction zone can be seen to contain elongate olivine crystals oriented normal to the orthopyroxene with abundant quench material. There does not appear to be any equilibrium clinopyroxene in the 2 GPa samples. However, it may be obscured by quench crystallization.

Textural features of CO_2-bearing dissolution experiments

At 1 GPa the short duration experiments show a thin rind of olivine and zoned clinopyroxene with interstitial pockets of glass (Table 4, Fig. 6c). At longer durations the reaction zone consists of olivine and clinopyroxene much of which is likely of quench origin.

In the 2 GPa experiments (Table 4, Fig. 6d) there are slightly smaller amounts of olivine than at 1 GPa, and clinopyroxene is more abundant, however, much of this may be due to quench crystallization. All of the interstitial material in these experiments consists of quench material with traces of interstitial glass. The occurrence of clinopyroxene in the CO_2-bearing experiments is in agreement with the equilibrium experiments.

Measurements of the thickness of the reaction zone in all the experiments regardless of volatile content indicate that the thickness of the visible zone is not sufficient to explain the observed amount of dissolution.

Chemical compositions

Chemical compositions were determined from the longest duration experiments (60 minutes +). The glass patches in the shorter duration experiments were too small to allow reliable analysis without overlap of the electron microprobe beam onto crystals or migration of alkalis. Quantitative analyses were obtained only for the 0.4 and 1 GPa anhydrous experiments and a 1 GPa hydrous experiment. Semi-quantitative analyses of the 1 GPa CO_2-bearing experiment and all the 2 GPa experiments were obtained by analyzing quench regions with a 10 to 20 μm diameter beam. The pristine nature of the glass in the 1 GPa hydrous experiment was unusual since these glasses are usually strongly affected by crystallization during quenching. To check that the glass was actually hydrous, several small chips were analyzed by FTIR. The absorption coefficient for glass of this composition is not known so the actual water content was not determined – only its presence. In the two samples checked in this way large peaks were obtained between 2700 and 3700 wavenumber indicating the presence of abundant water.

The composition of glass in the reaction zones and in the surrounding solvent melt is presented in Table 5 and shown graphically in Fig. 7. Compositions vary with pressure and volatile content. The reaction zone glass in 0.4 and 1 GPa anhydrous experiments and in the 1 GPa hydrous experiment shows a wide range of SiO_2 contents from 42 to 62 wt%. The range of SiO_2 in the 1 GPa CO_2-bearing experiment is more restricted (44–56%) and in all the experiments at 2 GPa all of the glass analyzed has less than 52 wt% SiO_2. The most SiO_2-rich glass in the anhydrous samples shows minor Na_2O enrichment over the solvent, and K_2O contents are more than double that in the solvent melt. The Si-enriched glass from the hydrous samples shows only minor Na_2O enrichment and in some cases even a small depletion relative to the original solvent but is strongly enriched in K_2O (Table 5). Glass from all the 2 GPa experiments is enriched in MgO relative to the solvent and the other more Si-rich glass. The high K_2O in the 2 GPa CO_2-bearing reaction zone glass may be a relic due to the extensive quench crystallization observed in these samples.

Comparison of the glass compositions in high pressure experiments with glasses formed at 1 atmosphere by basanite-orthopyroxene interaction (Shaw et al. 1998) shows that both the high pressure and low pressure data fall on generally similar trends although the degree of silica and Na_2O enrichment is less in the high pressure experiments and MgO tends to be higher. The MgO enrichment likely reflects the higher MgO content of the solvent used in this study.

The reaction zone glass in the 0.4 and 1 GPa dissolution experiments and those in hydrous experiments at 2 GPa show distinct similarities to natural Si-rich glasses found in mantle xenoliths (Fig. 7) except that the range of SiO_2 contents in the experiments is lower than in the natural samples and K_2O higher. The low Al_2O_3 in the experimentally produced glasses relative to those in nature may reflect the low Al content of the starting solvent or participation of an aluminous phase e.g., spinel, in the melt forming process in nature. The reaction zone glasses in the 2 GPa anhydrous and CO_2-bearing experiments are SiO_2 poor and do not compare favorably with xenolith glasses (Fig. 7).

Compositional profiles

Detailed profiles of glass composition were obtained for dry experiments at 0.4 and 1 GPa and for a 1 GPa hydrous experiment. These profiles are shown in Fig. 8. Note that the profiles have been shortened to bring out the details of the reaction zone; glass outside the reaction zone does not return to its original composition for at least 1 mm from the orthopyroxene.

Silica, TiO_2, FeO, CaO and P_2O_5 show the expected profile of decreasing SiO_2 with distance from the orthopyroxene. However, the SiO_2 contents are greater than possible by simple dissolution of orthopyroxene. In samples where clinopyroxene is present, the profiles show distinct breaks in slope across the clinopyroxene-rich region (Fig. 8). The transition from the olivine-bearing region of the reaction zone to the olivine-free solvent shows no break in slope. The pattern of Al_2O_3 is variable. At 0.4 GPa under anhydrous conditions Al_2O_3 decreases toward the orthopyroxene whereas at 1 GPa the concentration of Al_2O_3 increases slightly toward the orthopyroxene. This variation may reflect a change in the behavior of Al with increasing pressure. However, the presence of clinopyroxene in the reaction zone may also play a role in changing Al diffusion.

Given the Mg-rich orthopyroxene undergoing dissolution it might be expected that the reaction zone melt would be MgO rich and would show a profile of decreasing MgO with distance from the orthopyroxene, however, the release of large amounts of MgO during dissolution promotes olivine saturation and the reaction zone glasses actually are MgO poor compared with the solvent. Like Al_2O_3, Na_2O shows a generally flat pattern, however in all the profiles there is an enrichment of Na_2O in the most SiO_2-rich glass; this enrichment is more pronounced in the anhydrous experiments. There is extreme enrichment of K_2O in the glass adjacent to the orthopyroxene. The K_2O contents increase toward the orthopyroxene reaching maximum concentrations of 6.5 to 7 wt%.

Mineral compositions in reaction zones

Olivine and clinopyroxene compositions were measured in anhydrous, hydrous and CO_2-bearing samples (Table 6) in an attempt to decipher changes with run pressure and duration. There are no systematic variations in mineral composition as a function of time or of solvent composition. However, pressure appears to change the

Table 5 Representative glass compositions from dissolution experiments

Sample	97-op-4	97-op-4	97-op-4	97-op-4	97-op-4	97-op-9	97-op-9	97-op-9	97-op-9	97-op-9	97-op-9	97-op-14[a]	97-op-14[a]
P (GPa)	0.4	0.4	0.4	0.4	0.4	1	1	1	1	1	1	2	2
Volatile	None	None	None	None	None	None	None	None	None	None	None	None	None
SiO_2	61.69	60.53	48.60	46.11	42.12	58.96	57.95	56.28	46.51	44.10	42.70	47.61	44.35
TiO_2	0.40	0.31	1.93	2.04	2.83	0.71	0.70	0.79	2.46	2.32	2.64	1.74	2.41
Al_2O_3	9.59	7.70	10.75	11.07	12.24	11.92	12.30	13.56	11.89	11.46	11.33	11.28	10.41
FeO	5.29	5.50	8.53	8.66	10.65	5.58	4.50	4.65	9.27	9.25	11.12	7.76	9.73
MnO	0.11	0.00	0.14	0.08	0.10	0.10	0.06	0.13	0.15	0.18	0.20	0.2	0.08
MgO	5.77	7.67	5.51	5.37	7.30	6.27	6.45	6.48	5.42	9.63	10.71	8.58	14.26
CaO	4.32	5.23	14.38	15.54	15.73	4.81	5.23	6.33	14.73	14.09	14.60	10.22	11.68
Na_2O	3.47	4.00	3.21	3.09	2.75	4.39	3.48	3.37	3.80	3.01	2.57	4.33	1.09
K_2O	7.92	7.28	4.14	3.71	3.91	7.82	7.22	7.40	3.93	3.25	2.93	3.57	2.84
P_2O_5	0.05	0.00	0.60	0.64	0.92	0.07	0.05	0.08	0.88	0.86	0.95	0.42	0.48
Total	98.61	98.22	97.79	96.31	98.55	100.63	97.94	99.07	99.04	98.15	99.75	95.71	97.33
Sample	97-op-32	97-op-32	97-op-32	97-op-32	97-op-32	97-op-32	97-op-32	97-op-19b[a]	97-op-19b[a]	97-op-21a[a]	97-op-21a[a]	97-op-25[a]	97-op-25[a]
P (GPa)	1	1	1	1	1	1	1	2	2	1	1	2	2
Volatile	H_2O	H_2O	H_2O	H_2O	H_2O	H_2O	H_2O	H_2O	H_2O	CO_2	CO_2	CO_2	CO_2
SiO_2	59.58	54.48	52.02	52.02	46.37	45.26	43.94	51.65	50.25	50.76	44.27	48.04	45.35
TiO_2	1.31	1.38	1.66	1.66	1.72	2.14	2.21	1.27	1.39	1.90	2.39	1.62	2.08
Al_2O_3	12.56	12.92	13.52	13.52	9.14	9.93	10.50	8.54	8.30	14.22	10.89	10.47	13.32
FeO	6.76	6.94	7.07	7.07	8.66	9.27	9.48	6.20	7.04	8.37	10.71	8.60	9.91
MnO	0.18	0.14	0.09	0.09	0.22	0.17	0.18	0.13	0.13	0.16	0.22	0.22	0.19
MgO	1.83	2.95	1.62	1.62	11.81	11.97	11.63	14.70	16.63	4.37	9.53	11.84	7.78
CaO	2.55	1.94	5.27	5.27	12.09	11.62	12.36	11.12	10.30	7.08	10.13	9.73	5.95
Na_2O	2.51	2.53	2.85	2.85	2.60	2.42	2.41	2.16	1.80	3.43	2.88	2.72	3.22
K_2O	6.52	6.23	6.47	6.47	2.70	2.61	2.66	1.75	2.04	6.44	4.63	3.41	6.63
P_2O_5	0.25	0.42	0.73	0.73	0.72	0.79	0.85	0.49	0.41	0.58	0.84	0.35	0.51
Total	94.05	89.93	91.30	91.30	96.03	96.18	96.22	98.01	98.29	97.31	96.49	97.00	94.94

[a] These analyses should be considered semi-quantitative (see text for details)

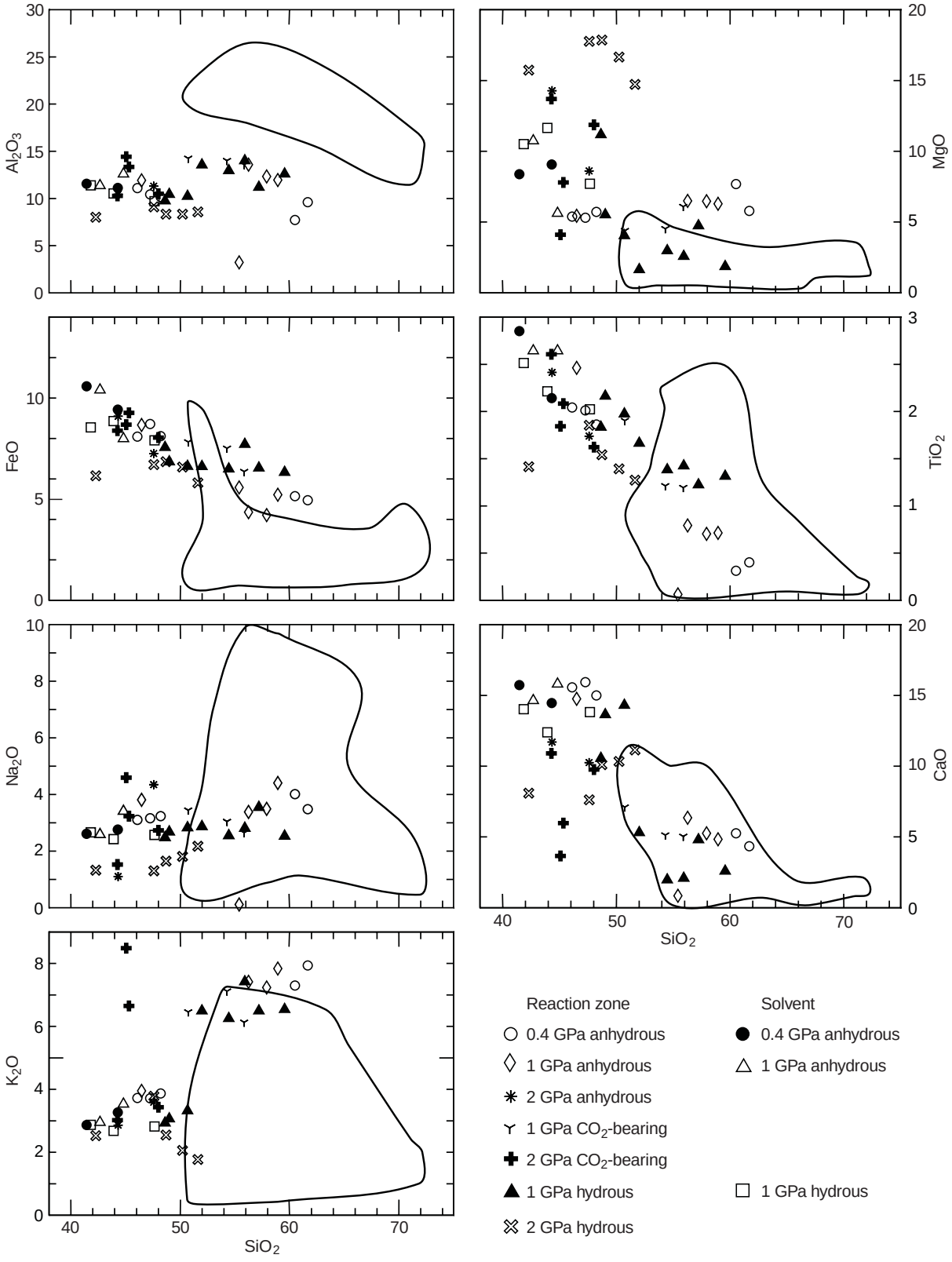

Fig. 7 Composition of reaction zone glass and solvent glass in the dissolution experiments. *Fields* give the range of composition of natural Si-rich alkaline glass inclusions from mantle xenoliths (see Fig. 1 for data sources)

CaO content of clinopyroxene; clinopyroxene from 0.4 and 1 GPa experiments is more calcic than those from 2 GPa experiments.

Olivine and clinopyroxene show distinct compositional variations across the reaction zones (Table 6). In

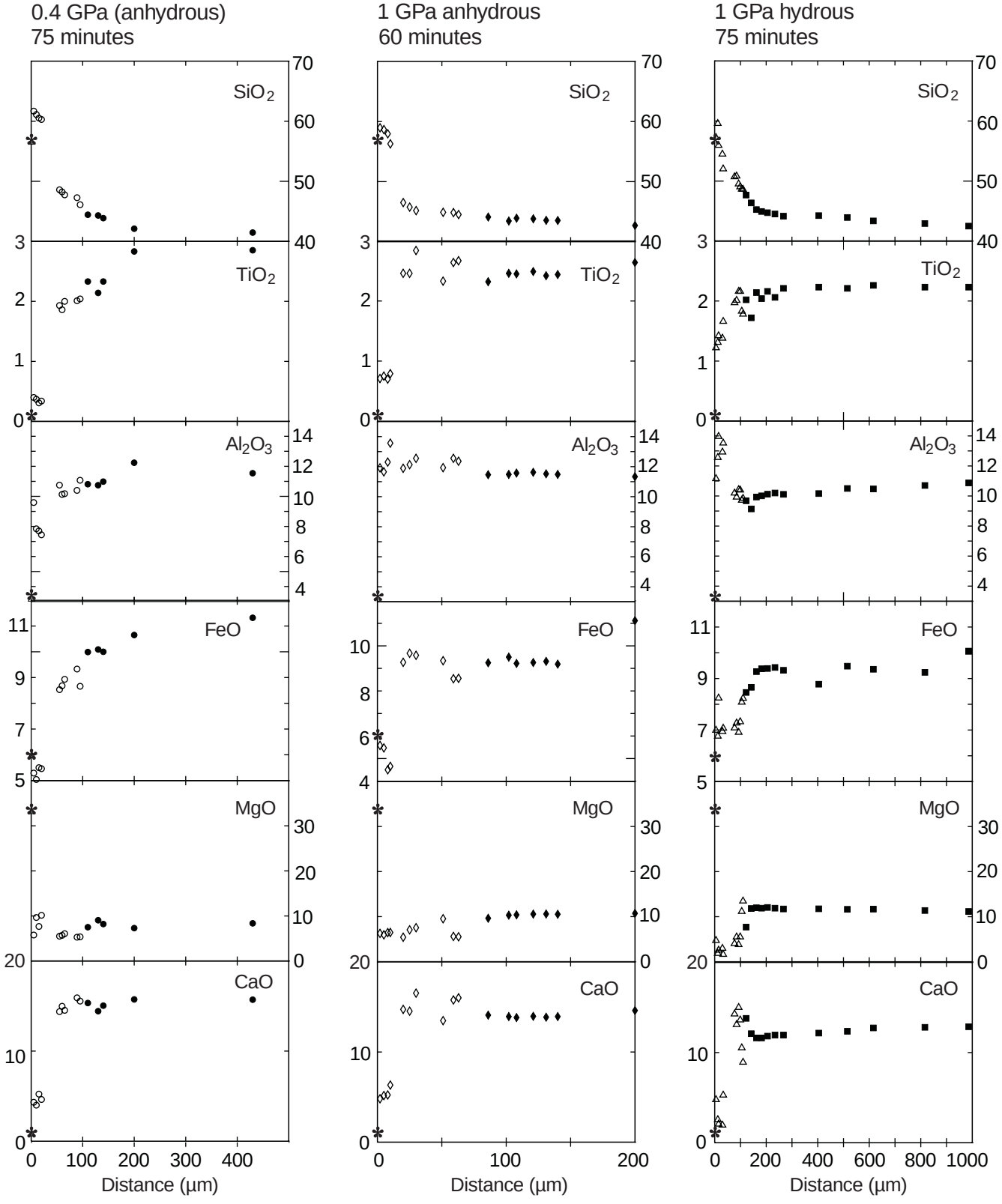

Fig. 8 Compositional variations with distance in reaction zones. The *change in symbol* on each plot shows the approximate edge of the visible reaction zone. The *asterisk* indicates the composition of the orthopyroxene undergoing dissolution

general the mg# [MgO/(MgO + FeO) × 100] of olivine decreases from the inner to the outer part of the reaction zone while CaO increases in the same direction. When present, clinopyroxene also shows a distinct variation in

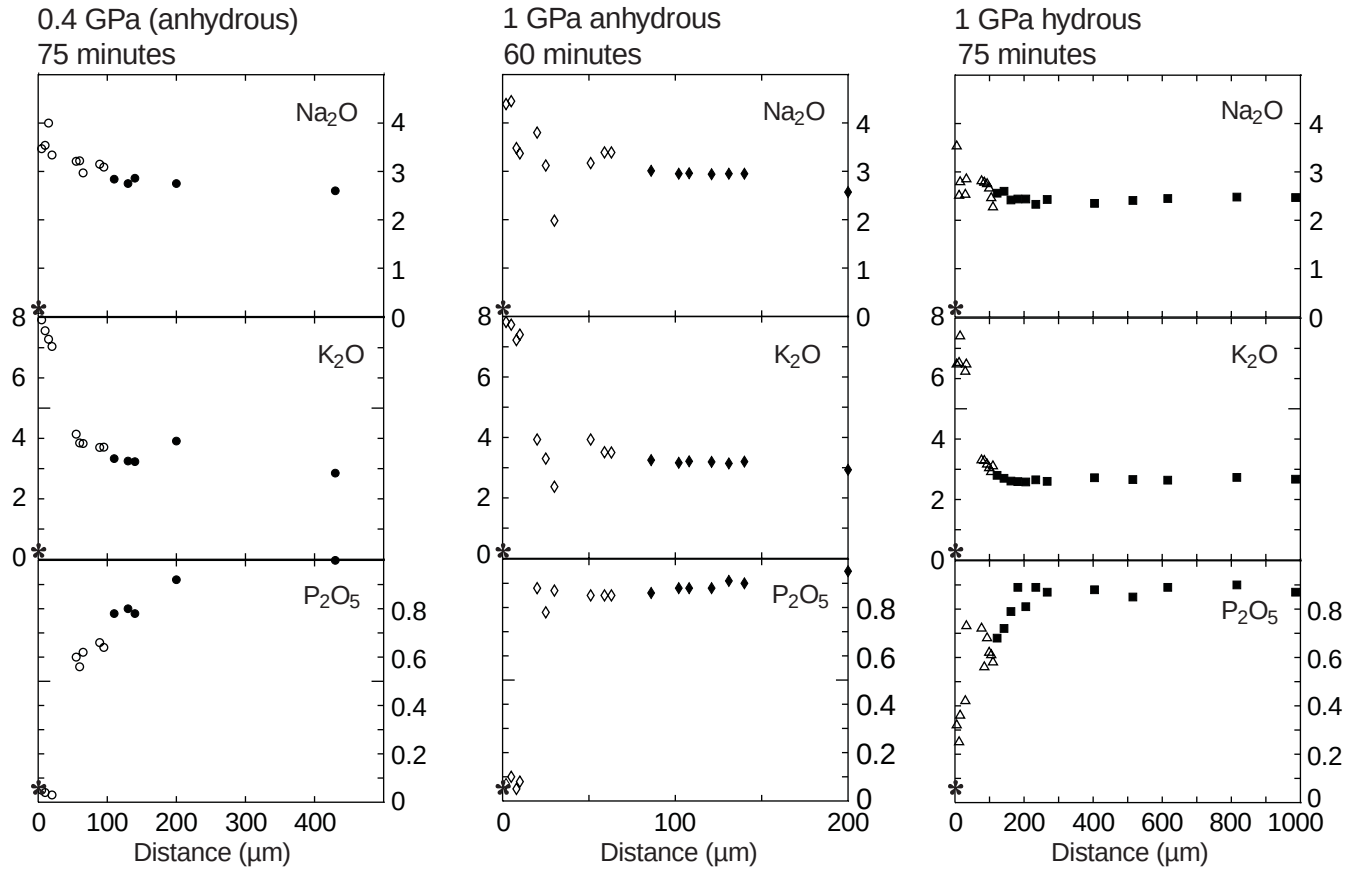

Fig. 8 (Continued)

composition from the inner faceted crystals to the outer ragged and rounded crystals. Oxides SiO_2, FeO, MgO and Na_2O decrease outward whereas TiO_2, Al_2O_3 and CaO increase.

Discussion

Comparison of natural and experimental glass compositions

Equilibration experiments produce secondary glasses that are slightly enriched in SiO_2 but not particularly alkali rich (Fig. 1). Thus, equilibration between orthopyroxene and infiltrating melt might be responsible for formation of some of the Si-enriched but alkali-poor glasses found in xenoliths but this mechanism does not appear to explain the extreme SiO_2 and alkali enrichment found in some xenolith glasses. Quench crystallization could lead to enrichments in SiO_2, Na_2O and K_2O in secondary melts, however Schiano and Clocchiatti (1994) found that melts in which the microlites had been redissolved gave extremely silica and alkali rich compositions suggesting that Si-rich glass inclusions represent true liquid compositions.

In contrast to the equilibration experiments, the secondary glasses formed during dissolution are both SiO_2 and alkali rich particularly at 0.4 and 1 GPa. Of the the 2 GPa dissolution experiments only those containing H_2O give Si-rich glass. This is in agreement with the results of Hirschmann et al. (1998) who suggested that there is strong pressure dependence of the activity of SiO_2 and that Si-rich melts likely do not exist at pressures greater than 1 GPa unless they are hydrous.

Although reaction between orthopyroxene and Si-undersaturated alkaline melt produces glass similar to that in xenoliths, these melts are transient and can only be preserved if the system is quenched prior to the attainment of equilibrium. If orthopyroxene-melt reaction takes place within the mantle there will be rapid equilibration leading to formation of an Si-enriched but relatively alkali-poor secondary melt. The only apparent way to preserve Si-rich glass with the extreme alkali enrichment seen in mantle xenolith glasses is to quench the reacting orthopyroxene-melt system prior to attainment of equilibrium. It is difficult to see how such equilibration could take place in the mantle. Transient Si-rich melts might also be transported away from the reaction zone before they reached equilibrium. At present there is insufficient data to assess such a model. The problem of quenching in disequilibrium melt compositions can be overcome if the reaction takes place during xenolith transport since the system will be quenched on eruption. Unless the transient Si-rich melts can be transported away from the reaction zone Si-rich glasses formed by this mechanism will have a distinct textural

Table 6 Composition of olivine and clinopyroxene from dissolution experiments [*mg*# MgO/(MgO + FeO)* 100]

Sample	97-op-4	97-op-10	97-op-10	97-op-10	97-op-10	97-op-10	97-op-10	97-op-12a	97-op-13a	97-op-15	97-op-32	97-op-19b	97-op-21a	97-op-23a	97-op-25
P (GPa)	0.4	1	1	1	1	1	1	2	2	2	1	2	1	1	2
Volatile	None	None	None	None	None	None	None	None	None	None	H_2O	H_2O	CO_2	CO_2	CO_2
Location[a]	–	42	51	84	100	144	177	–	–	–	–	–	–	–	–
Duration (min)	75	120	120	120	120	120	120	10	30	120	30	20	10	45	62
SiO_2	41.95	40.74	41.12	41.04	40.42	40.63	40.41	41.98	41.53	41.45	41.34	40.34	41.64	44.09	41.17
TiO_2	0.00	0.01	0.00	0.02	0.03	0.03	0.02	0.00	0.01	0.00	0.03	0.00	0.00	0.03	0.00
Al_2O_3	0.02	0.01	0.01	0.04	0.04	0.04	0.06	0.09	0.07	0.09	0.04	0.06	0.00	0.00	0.08
FeO	8.27	10.21	9.38	9.51	11.59	11.23	12.06	7.30	6.37	10.22	8.82	5.71	5.96	5.56	6.93
MnO	0.19	0.22	0.16	0.10	0.14	0.16	0.15	0.10	0.12	0.17	0.15	0.06	0.10	0.12	0.15
MgO	49.36	48.23	48.77	48.81	47.19	47.26	46.52	50.09	51.49	48.17	49.46	52.58	52.80	50.46	52.16
CaO	0.33	0.31	0.30	0.32	0.53	0.54	0.71	0.34	0.31	0.33	0.30	0.28	0.31	0.40	0.33
Na_2O	0.02	0.02	0.04	0.02	0.04	0.01	0.00	0.01	0.10	0.00	0.02	0.04	0.00	0.00	0.02
K_2O	0.03	0.01	0.00	0.00	0.01	0.01	0.01	0.00	0.00	0.00	0.01	0.02	0.00	0.00	0.00
Total	100.17	99.76	99.79	99.85	99.99	99.90	99.93	99.91	100.00	100.43	100.17	99.09	100.81	100.66	100.84
mg#	85.65	82.53	83.87	83.70	80.28	80.80	79.42	87.28	88.99	82.50	84.87	90.20	89.86	90.07	88.27

Sample	97-op-4	97-op-10	97-op-10	97-op-10	97-op-10	97-op-10	97-op-10	97-op-12a	97-op-14	97-op-15	97-op-32	97-op-19b	97-op-21a	97-op-25	97-op-25
P (GPa)	0.4	1	1	1	1	1	1	2	2	2	1	2	1	2	2
Volatile	None	None	None	None	None	None	None	None	None	None	H_2O	H_2O	CO_2	CO_2	CO_2
Location[a]	–	24	39	43	48	52	57	–	–		–	–	–	–	–
Duration (min)	75	120	120	120	120	120	120	10	60	120	30	20	10	62	62
SiO_2	55.09	55.19	53.36	54.19	54.81	52.91	53.24	55.89	52.47	56.67	54.37	51.11	53.26	54.50	54.14
TiO_2	0.12	0.14	0.33	0.18	0.18	0.44	0.34	0.15	0.38	0.13	0.14	1.12	0.31	0.27	0.26
Al_2O_3	0.47	1.02	1.93	1.28	1.11	2.25	1.87	3.16	3.82	1.41	1.10	6.30	3.24	2.75	3.52
FeO	3.09	4.34	3.28	3.48	3.75	3.44	3.52	4.36	3.87	5.64	4.50	7.32	3.95	4.25	3.90
MnO	0.05	0.08	0.03	0.06	0.12	0.13	0.10	0.09	0.17	0.17	0.06	0.15	0.02	0.16	0.11
MgO	19.77	22.46	18.16	19.19	20.77	17.31	17.88	24.01	19.71	27.33	23.90	17.68	20.05	24.88	22.46
CaO	19.80	15.56	21.56	20.28	18.31	22.49	21.89	11.94	17.32	8.16	14.10	14.05	18.29	12.20	14.11
Na_2O	0.52	0.54	0.50	0.51	0.55	0.39	0.42	1.00	0.76	0.49	0.44	1.35	0.65	0.69	0.69
K_2O	0.01	0.03	0.03	0.03	0.03	0.02	0.04	0.00	0.09	0.00	0.00	0.08	0.03	0.02	0.03
Total	98.92	99.36	99.20	99.21	99.64	99.39	99.29	100.60	98.59	100.00	98.61	99.16	99.80	99.72	99.22
mg#	86.48	83.81	84.68	84.64	84.69	83.41	83.56	84.63	83.59	82.89	84.15	70.72	83.54	85.41	85.20

[a] Distance from edge of orthopyroxene

association, i.e. with partly dissolved orthopyroxene, and olivine ± clinopyroxene.

Dissolution rates

Only one other study of orthopyroxene dissolution at high pressure has been carried out (Brearley and Scarfe 1986). Their study used a basalt solvent with 0.7% normative nepheline and gave dissolution rates much slower than those observed in the present study. The faster dissolution observed in the present study is due to the higher degree of Si-undersaturation of the basanite solvent (26% normative feldspathoids). The dissolution rates observed by Brearley and Scarfe (1986) were time independent and a reaction zone containing olivine was only observed in experiments at 0.5 GPa. In contrast orthopyroxene dissolution in basanite results in time dependent dissolution and development of reaction zones of olivine and in some cases clinopyroxene across the range of pressure studied.

Addition of volatiles to the solvent melt has a large effect on dissolution rate. Addition of 5% H_2O results in a large increase in the dissolution rate due to the higher diffusion rates generally associated with hydrous systems and the tendency for H_2O to depress the liquidus of the solvent melt.

In contrast, addition of 5% CO_2 to the basanite results in much slower dissolution. This suggests that although orthopyroxene is not in equilibrium with the solvent, it was closer to equilibrium than in the hydrous and anhydrous experiments. It is well known that addition of CO_2 to model peridotites increases the stability of enstatite (Eggler 1978) and it is likely that a similar effect occurs in the present experiments.

Pressure also affects dissolution rates. In the anhydrous and hydrous experiments dissolution rate increases with increasing pressure because diffusion is faster at high pressure than at low pressure. In the CO_2-bearing solvent the reverse is true; dissolution is faster at 1 GPa than at 2 GPa. This may reflect increasing stability of enstatite with increasing pressure in a CO_2-bearing system.

Dissolution mechanism

The following discussion concentrates mainly on the anhydrous experiments since the most information is available for these. In examining the mechanism of dissolution, several observations must be accounted for and explained. These are: the presence of olivine and in some experiments clinopyroxene, the time dependance of dissolution rate and the approximately constant thickness of the observed reaction zone.

Orthopyroxene may break down either incongruently to olivine plus a melt enriched in SiO_2 or congruently to a melt of orthopyroxene composition. In the simple system Fo-SiO_2 incongruent dissolution is limited to pressures below about 0.5 GPa and results in formation of about 6% olivine (Bowen and Andersen 1914; Kushiro et al. 1968). It is known that addition of water or alkalis can change the behavior of orthopyroxene and can extend the range of incongruent melting to much higher pressure (Kushiro et al. 1968; Kushiro 1975). The presence of 40–50% olivine in the reaction zones argues for incongruent melting of orthopyroxene. The high proportion of olivine formed is likely due to the high alkali content of the reaction zone melt (see below) which stabilizes olivine to a higher SiO_2 content than normal (Kushiro 1975).

Observation of time series experiments shows that in anhydrous experiments the reaction zones develop in two stages. In the first stage (up to 10 min) orthopyroxene dissolves in the solvent forming a secondary glass and olivine. In the second stage clinopyroxene appears in the inner part of the reaction zone indicating that diffusion of Ca inward toward the orthopyroxene has resulted in clinopyroxene saturation. This two-step process appears to explain the inflection of dissolution rates seen at approximately 10 minutes – the time at which clinopyroxene first appears. The presence of mineralogical zonation also explains the stepped compositional profiles in the reaction zone glass since clinopyroxene will act as a barrier to some cations thus changing diffusivities across the clinopyroxene-bearing zone.

Within the reaction zone under anhydrous conditions clinopyroxene is a transiently stable phase. It is precipitated from the reaction zone melt near the orthopyroxene where it is on the liquidus. Moving out from the orthopyroxene, clinopyroxene moves off the liquidus and begins to dissolve. Olivine is also only stable in the reaction zone. The decrease in olivine grain size outward is strongly suggestive that the outer part of the reaction zone is being progressively consumed by the surrounding solvent. This suggestion is supported by the observation that in general the reaction zone thickness is not large enough to account for the observed amount of dissolution. Thus, the major controls on dissolution rate are

1) Diffusion of components away from the interface;
2) Changing phase relations of the reaction zone melt.

The absence of clinopyroxene from the hydrous dissolution experiments may be due either to the higher amount of superheat available due to the depression of the liquidus by water or changes in the near liquidus phase relations of the reaction zone melt due to the presence of water.

Clinopyroxene is much more abundant in the reaction zones in the dissolution experiments with a CO_2-bearing solvent indicating that clinopyroxene is stabilized by addition of carbon dioxide. Olivine is less abundant since the addition of CO_2 to a melt tends to shrink the phase volume of olivine (Kushiro 1975).

Origin of Si-alkali-rich glass

Melt formed at the margin of a dissolving orthopyroxene is expected to be more SiO_2 rich than the liquid that is promoting dissolution. However, one would not expect to find the extreme K_2O and Na_2O enrichment nor the generally low MgO contents. The only source for alkalis is the solvent melt. Therefore, these must have diffused inward. Shaw et al. (1998) noted this behavior and suggested that it was due to the preference of alkalis for a Si-rich polymerized melt over Si-poor depolymerised melt as described by Watson (1982) and Ryerson and Hess (1978). The strong uphill diffusion noted particularly for K_2O and to a lesser degree for Na_2O indicates that for part of the experiment potassium and sodium were diffusing against their own concentration gradient. However, these components must have diffused down a chemical potential gradient as shown in Fig. 9. The effect seen here is similar to the "transient two-liquid equilibrium" noted by Watson (1982) and Watson and Jurewicz (1984). In this scenario two liquids of distinct composition in contact will mix via diffusion and attempt to establish equilibrium. The control on this process is mainly the diffusivity of the component of interest and the counter-diffusion required for charge balance. As noted by Watson and Jurewicz the main controlling component is likely SiO_2, which is the slowest diffusing species. The equilibrium is transient in that it exists only as long as the melts do not completely mix by diffusion.

It is well known that K_2O and Na_2O have a tendency to increase the phase volume of olivine and so lead to Si enrichment whereas TiO_2, P_2O_5, CO_2 and increasing pressure counteract this trend (Kushiro 1975). Hirschmann et al. (1998) have suggested that it is the enrichment in Na_2O and K_2O that lead to the formation of Si-rich low degree partial melts in peridotite. Orthopyroxene breakdown leads to the formation of a Si-rich layer around the crystal which in turn leads to inward diffusion of K and Na that will tend slightly to enrich the liquid in Si by the mechanism discussed by Kushiro (1975) and Hirschmann et al. (1998). There may be a feedback mechanism where a small enrichment in Si promotes diffusion of Na and K that in turn promote greater silica enrichment.

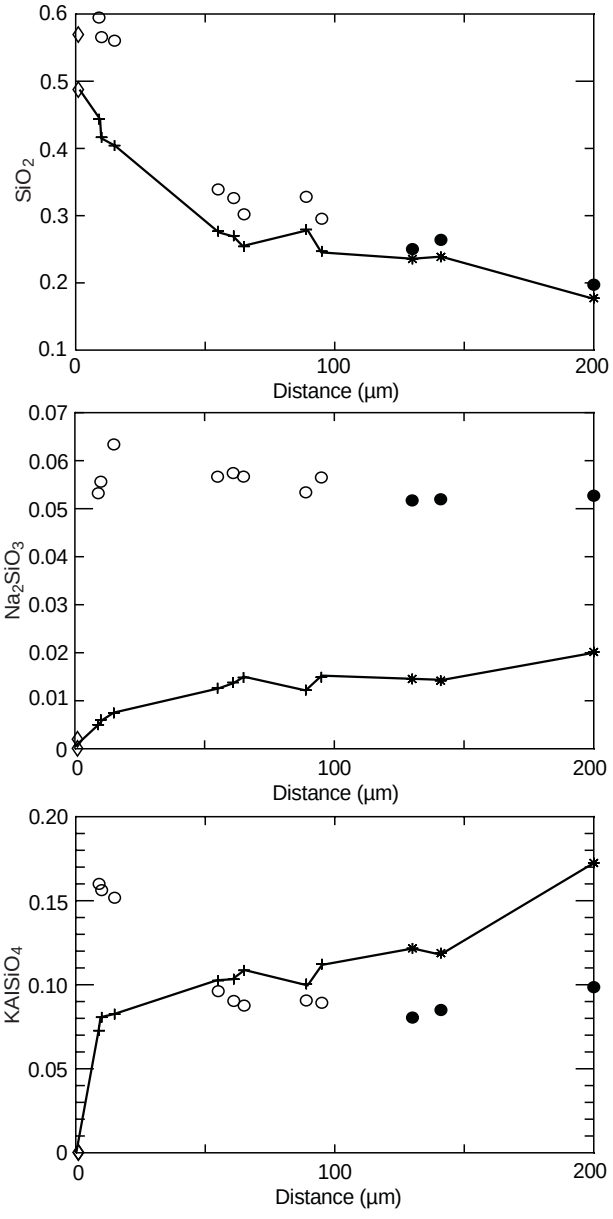

Fig. 9 Plot of mole fraction SiO_2, Na_2SiO_3 and $KAlSiO_4$ (*open and filled circles*) compared with calculated activity of these components in the reaction zone melts (*crosses and asterisks*) showing the decrease in silica activity outward from the dissolving orthopyroxene and the increase in Na_2SiO_3 and $KAlSiO_4$ activities outward from the orthopyroxene. It is these activity gradients (and thus chemical potential gradients) that permit the inward diffusion of Na and K. Activities were calculated using the MELTS supplemental calculator (Ghiorso and Sack 1995)

Effect of pressure and volatile content on reaction zone glass composition

The present experiments show that the formation of Si-rich glass is most likely to occur at pressures of 1 GPa or less. The presence of water extends the pressure range over which Si-rich melts can form to 2 GPa by expanding the phase volume of olivine. The presence of CO_2 decreases dissolution rates and in general decreases the Si content of the melt by shrinking the phase volume of olivine as suggested by Kushiro (1975). Since these liquids are less Si rich, they are thus less polymerized and K and Na do not show such a strong preference for them. In anhydrous and CO_2-bearing experiments at 2 GPa the glasses are not Si enriched because increasing pressure tends to shrink the olivine phase volume and thus lead to less Si-rich melts. Additionally stabilization of clinopyroxene in larger amounts than olivine will tend to decrease the Si content of the reaction zone melt and thus there will be less Na and K diffusion and so less secondary Si enrichment.

Effect of orthopyroxene on the solvent melt

In these experiments the contaminated zone reaches 100 to 300 microns outside the visible reaction zone however, with increasing distance from the dissolving orthopyroxene the composition of the solvent gradually approaches that of the starting solvent. This was not the case in the 1 atmosphere experiments described by Shaw et al. (1998). In this work the bulk contamination of the solvent was attributed to compositional convection (mixing) between the reaction zone and the solvent perhaps caused by density contrasts between reaction zone and solvent. The absence of bulk contamination in the present experiments argues against such a process since the reaction zones are similar in all respects to those seen at 1 atmosphere. Instead the bulk mixing at 1 atmosphere may have been an experimental artifact perhaps due to mixing induced by bubble migration or to the presence of a free liquid surface in the experiments.

The decrease of olivine grain size in many of the reaction zones and the qualitative observations that the reaction zone is never thick enough to explain all the observed dissolution suggests that the reaction zone must be removed by some process. The decrease in olivine grain size with increasing distance from the orthopyroxene interface suggests that the outer part of the reaction zone may progressively dissolve as the orthopyroxene interface moves inward.

Concluding remarks

The experiments reported here have shown that only a very small proportion of Si-rich alkaline melts are likely to be produced under equilibrium conditions by reaction of orthopyroxene and Si-undersaturated melt under conditions comparable to those in the upper mantle. However, dissolution experiments show that if the system is quenched prior to attainment of equilibrium the secondary glasses formed closely match the extreme compositions of glass in mantle xenoliths at pressures of 0.4 and 1 GPa. The presence of water extends the range over which Si-enriched glass will form to 2 GPa. These results suggest that orthopyroxene-melt reaction in situ within the mantle is likely not a viable origin for these extreme glass compositions if it leads to equilibration. Instead, it seems that reaction during transport of the xenoliths to surface is likely but the secondary melts formed in this way will have a specific textural association. Thus the Si-Al-rich alkaline glass inclusions trapped in mantle minerals (e.g. Schiano and Clocchiatti 1994) appear to have a different origin. However, many of the large interconnected veins and pools of melt may have formed by reaction processes during ascent. Thus, if we wish to understand the nature of the metasomatic agent in the mantle we must confine our studies to completely isolated glass inclusions since veins and pools will undoubtedly show the effects of assimilation.

Dissolution experiments reacting orthopyroxene with basanite melt under anhydrous, hydrous and CO_2-bearing conditions at pressures between 0.4 and 2 GPa result in variably thick reaction zones consisting of olivine, glass ± clinopyroxene. The occurrence of clinopyroxene is time dependant and is the reason for the time dependence of dissolution rates in the anhydrous experiments. Clinopyroxene is transiently stable within the reaction zones. Dissolution rates in hydrous experiments are much faster than under dry conditions. The presence of CO_2 in the solvent melt slows dissolution.

The composition of glass in the reaction zone varies with distance from the orthopyroxene and as a function of pressure and volatile content. All of the experiments at 0.4 and 1 GPa result in formation of SiO_2-rich alkaline glasses similar to those found in mantle xenoliths. However, Si contents are lower for glasses formed in the presence of CO_2. At 2 GPa glasses are only slightly enriched in SiO_2 and do not show large concentrations of alkalis. The alkalis are enriched in the reaction zone due to their preference for polymerized melt over poorly-polymerized melt. The enrichment of alkalis leads to crystallisation of a large amount of olivine and thus enrichment in SiO_2 over that expected for simple dissolution of orthopyroxene since alkalis increase the phase volume of olivine (Kushiro 1975).

Melt compositions in equilibrium experiments are distinct from those in reaction zones in that they have lower SiO_2, Na_2O and K_2O. This suggests that if orthopyroxene-melt reaction occurs in the mantle there must be a mechanism by which Si-rich melt formed at the margin of the dissolving orthopyroxene is removed.

The present database (Shaw et al. 1998 and this study) indicates that orthopyroxene-melt reaction is a viable mechanism for the formation of SiO_2-rich alkaline melts in mantle xenoliths either in situ immediately prior to entrainment or during emplacement. Detailed petrographic studies such as that presented by Wilshire and McGuire (1996) and Neumann and Wulff-Pedersen (1997) are required to determine at what point melt infiltration occurred.

Acknowledgements This paper is dedicated to the memory of Professor Alan Edgar. Thanks to Tatsu Kawamoto for donating part of his San Carlos xenolith collection, Detlef Krausse for his help with the electron microprobe, G. Herrmannsdörfer and H. Fischer for preparing sample assemblies for the piston cylinder and Steve Mackwell for the FTIR analyses and discussions on possible mechanisms for trapping glass inclusions. Thorough and constructive reviews by G. Yaxley and an anonymous reviewer are greatly appreciated.

References

Bond WL (1951) Making small spheres. Rev Sci Instrum 22: 344–345

Bowen NL, Andersen O (1914) The binary system MgO-SiO_2. Am J Sci 37: 447–500

Brearley M, Scarfe CM (1986) Dissolution rates of upper mantle minerals in an alkali basalt melt at high pressure: an experi-

mental study and implications for ultramafic xenolith survival. J Petrol 27: 1157–1182
Dautria JM, Dupuy C, Takherist D, Dostal J (1992) Carbonate metasomatism in the lithospheric mantle: peridotite xenoliths from a melilititic district of the Sahara basin. Contrib Mineral Petrol 111: 37–52
Donaldson CH (1985) A comment on crystal shapes resulting from dissolution in magmas. Mineral Mag 49: 129–132
Draper DS (1992) Spinel lherzolite xenolith from Lorena Butte, Simcoe Mountains, Southern Washington (USA). J Geol 100: 766–776
Edgar AD, Arima M, Baldwin DK, Bell DR, Shee SR, Skinner MW, Walker EC (1988) High pressure-high temperature melting experiments on a SiO_2-poor aphanitic kimberlite from the Wesselton mine, Kimberly, South Africa. Am Mineral 73: 524–533
Edgar AD, Lloyd FE, Forsyth DM, Barnett RL (1989) Origin of glass in upper mantle xenoliths from the Quaternary volcanics of Gees, West Eifel, Germany. Contrib Mineral Petrol 103: 277–286
Eggler DH (1978) The effect of CO_2 upon partial melting of peridotite in the system Na_2O-CaO-Al_2O_3-MgO-SiO_2-CO_2 to 35 kbar with an analysis of melting in a peridotite-H_2O-CO_2 system. Am J Sci 278: 305–343
Francis DM (1976a) The origin of amphibole in lherzolite xenoliths from Nunivak Island, Alaska. J Petrol 17: 357–378
Francis DM (1976b) Amphibole pyroxenite xenoliths: cumulate or replacement phenomena from the upper mantle, Nunivak Island, Alaska. Contrib Mineral Petrol 58: 51–61
Francis DM (1987) Mantle-melt interaction recorded in spinel lherzolite xenoliths from the Alligator Lake Volcanic Complex, Yukon, Canada. J Petrol 28: 569–597
Frey FA, Green DH (1974) The mineralogy, geochemistry and origin of lherzolite inclusions in Victoria basanites. Geochim Cosmochim Acta 38: 1023–1059
Gamble JA, Kyle PR (1987) The origins of glass and amphibole in spinel-wehrlite xenoliths from Foster Crater, McMurdo Volcanic Group, Antarctica. J Petrol 25: 755–779
Ghiorso MS, Sack RO (1995) Chemical mass transfer in magmatic processes. IV. A revised and internally consistent thermodynamic model for the interpolation and extrapolation of liquid–solid equilibria in magmatic systems at elevated temperatures and pressures. Contrib Mineral Petrol 119: 197–212
Hansteen TH, Andersen T, Neumann E-R, Jelsma H (1991) Fluid and silicate glass inclusions in ultramafic and mafic xenoliths from Hierro, Canary Islands: implications for mantle metasomatism. Contrib Mineral Petrol 107: 242–254
Hauri EH, Shimizu N, Dieu JJ, Hart SR (1993) Evidence for hotspot-related carbonatite metasomatism in the oceanic upper mantle. Nature 365: 221–227
Hirschmann MM, Baker MB, Stolper EM (1998) The effect of alkalis on the silica content of mantle-derived melts. Geochim Cosmochim Acta 62: 883–902
Holland TJB (1980) The reaction albite = jadeite + quartz determined experimentally in the range 600–1200. Am Mineral 65: 129–134
Ionov DA, Dupuy C, O'Reilly SY, Kopylova MG, Genshaft YS (1993) Carbonated peridotite xenoliths from Spitzbergen: implications for trace element signature of mantle carbonate metasomatism. Earth Planet Sci Lett 119: 283–297
Ionov DA, Hofmann AW, Shimizu N (1994) Metasomatism-induced melting in mantle xenoliths from Mongolia. J Petrol 35: 753–785
Jones AP, Smith JV, Dawson JB (1983) Glasses in mantle xenoliths from Olmani, Tanzania. J Geol 91: 167–178
Kelemen PB (1986) Reaction between ultramafic rock and fractionating basaltic magma. I. Phase relations, the origin of calc-alkaline magma series and the formation of discordant dunite. J Petrol 31: 51–98
Klügel A (1998) Reactions between mantle xenoliths and host magma beneath La Palma (Canary Islands): constraints on magma ascent rates and crustal reservoirs. Contrib Mineral Petrol 131: 237–257
Kushiro I (1975) On the nature of silicate melt and its significance in magma genesis: regularities in the shift of the liquidus boundaries involving olivine, pyroxene and silica minerals. Am J Sci 275: 411–431
Kushiro I, Yoder HS, Nishikawa M (1968) Effect of water on the melting of enstatite. Geol Soc Am Bull 79: 1685–1692
Navon O, Stolper E (1987) Geochemical consequences of melt percolation – the upper mantle as a chromatographic column. J Geol 95: 285–307
Neumann E-R, Wulff-Pedersen E (1997) The origin of highly silicic glass in mantle xenoliths from the Canary Islands. J Petrol 38: 1512–1539
O'Connor TK, Edgar AD, Lloyd FE (1996) Origin of glass in Quaternary mantle xenoliths from Meerfeldermaar, West Eifel, Germany: implications for enrichment in the lithospheric mantle. Can Mineral 34: 187–200
Reiners PW (1998) Reactive melt transport in the mantle and geochemical signatures of mantle-derived magmas. J Petrol 39: 1039–1061
Ryerson FJ, Hess PC (1978) Implication of liquid-liquid distribution coefficients to mineral-liquid partitioning. Geochim Cosmochim Acta 42: 921–932
Schiano P, Clocchiatti R (1994) Worldwide occurrence of silica-rich melts in sub-continental and sub-oceanic mantle minerals. Nature 368: 621–624
Schiano P, Clocchiatti R, Shimizu N, Weis D, Mattielli N (1994) Cogenetic silica-rich and carbonate-rich melts trapped in mantle minerals in Kerguelen ultramafic xenoliths: implications for metasomatism in the oceanic upper mantle. Earth Planet Sci Lett 123: 167–178
Schiano P, Clocchiatti R, Shimizu N, Maury RC, Jochum KP, Hofmann AW (1995) Hydrous silica-rich melts in the sub-arc mantle and their relationship with erupted arc lavas. Nature 377: 595–600
Shaw CSJ, Edgar AD (1997) Post-entrainment mineral-melt reactions in spinel peridotite xenoliths from Inver, Donegal, Ireland. Geol Mag 134: 771–779
Shaw CSJ, Thibault Y, Edgar AD, Lloyd FE (1998) Mechanisms of orthopyroxene dissolution in silica-undersaturated melts at 1 atmosphere and implications for the origin of silica-rich glass in mantle xenoliths. Contrib Mineral Petrol 132: 354–370
Thibault Y, Holloway JR (1994) Solubility of CO_2 in a Ca-rich leucitite: effects of pressure, temperature and oxygen fugacity. Contrib Mineral Petrol 116: 216–224
Tracy RJ (1980) Petrology and significance of an ultramafic xenolith suite from Tahiti. Earth Planet Sci Lett 48: 80–96
Watson EB (1982) Basalt contamination by continental crust: some experiments and models. Contrib Mineral Petrol 80: 73–87
Watson EB, Jurewicz SR (1984) Behaviour of alkalis during diffusive interaction of granitic xenoliths with basaltic magma. J Geol 92: 121–131
Wilshire HG, McGuire AV (1996) Magmatic infiltration and melting in the lower crust and upper mantle beneath the Cima volcanic field, California. Contrib Mineral Petrol 123: 135–374
Wulff-Pedersen E, Neumann E-R, Jensen BB (1996) The upper mantle under La Palma, Canary Islands: formation of Si-K-Na-rich melt and its importance as a metasomatic agent. Contrib Mineral Petrol 125: 113–139
Yaxley GM, Kemenetsky V, Green DH, Falloon TJ (1997) Glasses in mantle xenoliths from western Victoria, Australia, and their relevance to mantle processes. Earth Planet Sci Lett 148: 433–446
Zinngrebe E, Foley SF (1995) Metasomatism in mantle xenoliths from Gees, West Eifel, Germany: evidence of calc-alkaline glasses and metasomatic Ca-enrichment. Contrib Mineral Petrol 122: 79–96